One-Pot Electrochemical Exfoliation of Graphene Oxide in Nanofibrillated Kenaf Cellulose (NFC) for the Development of Conductive Paper

Tretya Ardyani[1], Azmi Mohamed[1,2*], Suriani Abu Bakar[2], Masanobu Sagisaka[3], Yasushi Umetsu[3] Mohamad Hafiz Mamat[4], Mohd Khairul Ahmad[5], H.P.S. Abdul Khalil [6] Stephen King[7], Sarah E. Rogers[7], Julian Eastoe[8]

[1]Department of Chemistry, [2]Nanotechnology Research Centre, Faculty of Science and Mathematics, Universiti Pendidikan Sultan Idris, 35900 Tanjong Malim, Perak, Malaysia

[3]Department of Frontier Materials Chemistry, Graduate School of Science and Technology, Hirosaki University, Bunkyo-cho 3, Hirosaki, Aomori 036-8561, Japan

[4]NANO-SciTech Centre (NST), Institute of Science (IOS), Universiti Teknologi MARA (UiTM), 40450 Shah Alam, Selangor, Malaysia

[5]Microelectronic and Nanotechnology – Shamsuddin Research Centre (MiNT-SRC), Faculty of Electrical and Electronic Engineering, Universiti Tun Hussein Onn Malaysia, 86400 Parit Raja, Batu Pahat, Johor, Malaysia

[6]School of Industrial Technology, Universiti Sains Malaysia, 11700 Gelugor, Penang, Malaysia

[7]Rutherford Appleton Laboratory, ISIS Spallation Source, Chilton, Oxfordshire, OX110QT, United Kingdom

[8]School of Chemistry, University of Bristol, Cantock's Close, Bristol, BS8 1TS, United Kingdom

*Corresponding author. Tel.: +601548797582; fax: +601548797296

Abstract

The effect of incorporating common dodecyl anionic and cationic surfactants such as dodecyltrimethylammonium bromide (DTAB), dodecylethyldimethylammonium bromide (DDAB), and sodium dodecylsulfate (SDS) in nanocomposites of reduced graphene oxide and nanocellulose are described. The stabilization and electrical properties of the nanocomoposites of reduced graphene oxide (RGO) and nanofibrillated kenaf cellulose (NFC) were characterized using four-point probe electrical conductivity measurements. Raman spectroscopy, field emission scanning electron microscopy, and high-resolution transmission electron microscopy were used to investigate dispersion morphology and quality RGO inside the NFC matrices. Small-angle neutron scattering (SANS) was used to study the aggregation behavior of the surfactant aqueous systems and RGO dispersions. The cationic surfactant DTAB proved to be the best choice for stabilization of RGO in NFC, giving enhanced electrical conductivity of five orders of magnitude higher than the neat NFC. The results highlight the effects of hydrophilic surfactant moieties on structure, stability and properties of RGO/NFC composites.

Keywords: ionic surfactant, reduced graphene oxide, electrochemical exfoliation, conductive paper, nanocellulose

1. Introduction

There is a strong drive for using nanocellulose in the development of polymer nanocomposites, which offer various benefits including low environmental impact. Recently researchers have been attempting to incorporate graphene into nanocellulose matrices for applications requiring good electrical properties, such as conducting papers (Hou, Xu, & Li, 2018; Wang, Bian, Ji, & Yang, 2018). The most common approach to fabricate graphene/nanocellulose paper is by blending, where the electrical conductivity of the resulting composite is highly dependent on the amount of incorporated graphene and the dispersion quality (Nguyen Dang & Seppälä, 2015; Peng, Meng, Niu, & Lu, 2012; Wang, Drzal, Qin, & Huang, 2015). Numerous studies on graphene/nanocellulose papers have reported remarkable electrical conductivities. Wang et al. a conductivity of 1.98 x 10^{-1} S cm^{-1} with a graphene content of 20 wt% (Wang et al., 2018). Previously Ye et al. (2016) also noted similar conductivities (1.50 x 10^{-1} S cm^{-1}), albeit with a higher graphene content (50 wt%). Xiong et al. (2016) claimed to reach an electrical conductivity of nearly 50 S cm^{-1} with nanocellulose/graphene oxide nanomembranes at 56.8 wt% graphene content.

One of the merits of nanocomposite-reinforced by graphene is the possibility of reaching high and stable electrical conductivities. Problems arise however, because of the difficulty of dispersing graphene in nanocellulose. Furthermore, improving the dispersibility of nanocellulose in aqueous phases is also particularly challenging. Although the aforementioned studies have reported highly conductive graphene/nanocellulose papers, high filler loadings are required, having negative economic and environmental impacts. In most cases, surface modifications are

required, or added electrolytes or alkaline conditions are necessary to achieve stable nanocellulose systems (Zhang, Liu, Zheng, & Zhu, 2012; Zhou & Zhang, 2000). Functionalization of graphene is also commonly used to overcome the challenges of stabilizing dispersions (Georgakilas et al., 2012). Although nanocellulose itself is considered an environmentally safe material, chemical functionalization can compromise this advantage. On the other hand, chemical functionalization of graphene can be expected to affect the π-conjugated network responsible for distributing electrical flow (Mohamed et al., 2016). Therefore, in an effort to seek an economical and effective approach, the focus here is on the use of added surfactants to help improve compatibility between graphene and nanocellulose.

As such, surfactants can be considered as an appealing alternative and numerous articles have discussed this approach for enhancing surface properties of graphene and carbon nanotubes (Mohamed et al., 2016; Tkalya, Ghislandi, de With, & Koning, 2012). The same concept could be useful for nanocellulose-graphene composites. Our previous work introduced a simple method for obtaining stable graphene/nanocellulose dispersions with the help of ionic liquid type surfactants (Mohamed et al., 2018a). The resulting dispersions can be further cast to generate graphene/nanocellulose conductive papers. Applying similar concepts, and to explore surfactants that are compatible with both graphenes and nanocellulose, the focus here is shifted to cationic surfactants. Since the first report of surfactants for graphene processing emerged, various types have been tested (Lin et al., 2016; Mohamed et al., 2016; Tkalya et al., 2012). Most studies use anionic surfactants, whereas works with cationic surfactants are more limited. In early research, a range of quaternary ammonium cationic surfactants were used to prepare surfactant-intercalated graphite AZMI IS IT GRAPHITE OR GRAPHENE – CHECK AND CORRECT THIS? oxide

(Matsuo, Niwa, & Sugie, 1999). They reported an ability to control interlayer spacing by changing the surfactant type and concentration. Fourier transform infrared (FTIR) spectroscopy results suggested intermolecular interactions between surfactants and the oxygens of graphite oxide. Later, others demonstrated successful exfoliation of graphite assisted by cetyltrimethylammonium bromide (CTAB) to yield few layered graphene sheets (Vadukumpully, Paul, & Valiyaveettil, 2009). In a different study, this surfactant was observed to increase dispersion quality of reduced graphene oxide (RGO) in natural rubber latex (NRL) matrices through conventional mixing. Enhancements of several properties were claimed, although the electrical conductivity was only moderately improved (Matos, Galembeck, & Zarbin, 2014).

Regarding studies with nanocellulose, the majority of surfactants studied are anionic and nonionic (Tardy et al., 2017). A comprehensive understanding of how ionic surfactants affect physicochemical properties would, therefore, underpin the knowledge of the structure–performance relationships of ionic surfactants. To date, despite limited examples (Tardy et al., 2017), literature reports of systematic studies comparing anionic and cationic surfactants for composites of graphene and nanocellulose still remain scarce. This current study investigates how interfacial interactions, system stabilization and physicochemical properties are influenced by choice of surfactant. Two different cationic surfactants are investigated here, both bearing C12 hydrophobic chains (Table 1): dodecyltrimethylammonium bromide (DTAB) and dodecylethyldimethylammonium bromide (DDAB). From the quaternary ammonium series, DDAB would be the most appropriate to benchmark the performance of DTAB as these surfactants only differ by substitution of a methyl group on DTAB with a longer ethyl chain on the polar head. To provide a comparable alternative, the C12 chain anionic sodium dodecylsulfate (SDS) is also included in the

study. The results will help to identify efficient commercially available cationic and ionic surfactants for nanocellulose-graphene composites.

Table 1

Chemical structures of surfactants used in this study

Abbreviation	Chemical structure and name
DTAB	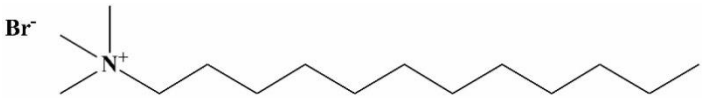 Dodecyltrimethylammonium bromide
DDAB	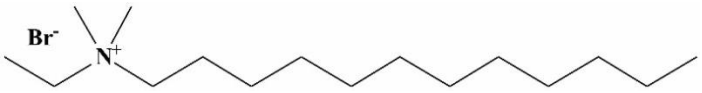 Dodecylethyldimethylammonium bromide
SDS	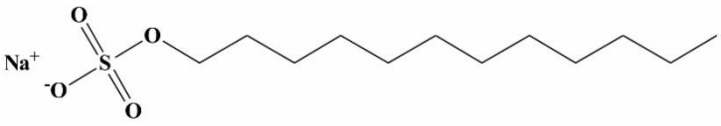 Sodium dodecylsulfate

2. Materials and methods

2.1 Materials

Dodecyltrimethylammonium bromide (DTAB) and Dodecylethyldimethylammonium bromide (DDAB) were purchased from Acros Organics and used without further purification. Sodium dodecylsulfate (SDS; Systerm) was used as received. Nanofibrillated kenaf cellulose was a gift from the Forest Research Institute Malaysia. Graphite rods with diameter of 10 mm and length of 150 mm were obtained from Goodfellow, GmBH. Hydrazine hydrate was obtained from Merck and used as received.

2.2 Preparation of Graphene/Nanofibrillated Kenaf Cellulose (NFC) Conductive Paper (GCP)

2.5 g of NFC was first dispersed in surfactant solutions (0.500, 0.200, 0.100, 0.075 and 0.050 M) to obtain 50 mL NFC/surfactant dispersions. The mixtures were then vigorously stirred for 2 hours to form stable dispersions. The surfactant/NFC dispersions were then used as electrolyte for the exfoliation of graphene at a constant voltage of 7V (GW INSTEK GPS 303000) with graphite rods as both electrodes. The electrochemical exfoliation was carried out at room temperature for 24 hours. Next the dispersions were subjected to mechanical stirring and sonication for 1 hour, resulting in homogeneous mixtures of graphene oxide (GO)/NFC/surfactant. For the reduction of graphene hydrazine hydrate (0.1 mL hydrazine /10 mL GO dispersion) was used and the reaction was carried out under reflux at 90 – 100 °C for 24 hours. After the reaction was completed, the mixture was then filtered and dried overnight on a filter paper in an oven at 50 °C. Dark to light grey papers (GCP) were obtained by peeling the papers from filter paper substrates. The amount of nanofiller in the GCPs is given in Table S1.

2.3 Preparation of NFC/Surfactant Composites

The NFC/surfactant dispersions (50 mL) were obtained by dispersing 2.5 g of NFC in surfactant solutions with vigorous stirring for 2 hours to form stable dispersions. The mixtures were then filtered and dried overnight on a filter paper in an oven at 50 °C. Similar to the GCP, the NFC/surfactant composites were obtained after peeling the resulting papers off from the filter paper substrates.

2.4 GCP Characterization

The electrical conductivities of GCPs were measured by a four-point probe method (Keithley 2636A). The morphologies and microstructure of GCPs were observed under a field emission electron microscope (FESEM, Hitachi SU8020). Raman spectroscopy was carried out using a Renishaw InVia micro Raman system spectrophotometer with a 514 nm argon-ion laser source. To visualize the embedded microstructures of nanocellulose papers, high resolution transmission electron microscopy (HRTEM JEOL 2100F) was used. Prior to HRTEM imaging, the GCPs were cryo-ultramicrotomed with a diamond knife to give sections with nominal thickness ~80 nm.

2.5 Zeta potential measurements

Zeta potential measurements were performed using a ELSZ-1000 Zeta-potential and Particle Size Analyzer (Photal Otsuka Electronics) employing the Smoluchowski equation and 1 peak Lorentz fitting. Measurements were carried out with a flow cell at a sampling time of 400 μs, cumulative number 7, measuring angle 15º, temperature 25 ºC, pin hole size 50 μm, and cell constant 70.000 cm^{-1}. Properties of aqueous mixtures including refractive index of 1.3328, viscosity of 0.8878 cP, and dielectric constant of 78.3 were used for calculation of zeta potential. Zeta potential values were finally obtained as average values of 10 runs for each sample.

2.6 Small-angle neutron scattering (SANS)

Small-angle neutron scattering (SANS) studies were carried out on the time-of-flight LOQ instrument at ISIS, UK. The accessible *Q* range was 0.007 – 0.23 $Å^{-1}$, arising from incident neutron wavelengths of λ = 2.2 – 10 Å. Absolute intensities for *I(Q)* (cm^{-1}) were determined to within 5% by measuring the scattering from a partially

deuterated polymer standard. The samples were prepared in 2 mm path-length quartz cells and held in a thermostatted automatic sample changer at 25°C. Data have been fitted using the SASView interactive fitting program by fixing scattering length densities and known parameters as constant values. Unknown structural parameters were allowed to float during the fitting process to obtain an optimized fit as required by the different scattering laws.

3. Results and discussion

3.1 Electrical properties of graphene/NFC paper (GCP)

Greyish papers disk having diameters of 6.50 – 6.57 cm and 0.14 – 0.18 mm in thickness were obtained. The four-probe electrical conductivities of the papers at room temperature are summarized in Table 2. The relationship between electrical conductivity achieved by GCPs and surfactant concentration, on the other hand, is depicted in Fig. S1. As expected, the use of surfactants for improving RGO dispersion inside the NFC matrices leads to enhancements in electrical properties of NFC paper. Comparisons between samples with and without RGO clearly show that this is due to the presence of RGO dispersed in NFC matrix.

Table 2

Electrical conductivities of NFCs with and without RGO stabilized by surfactants

Sample	Surfactant concentration (M)				
	0.050	**0.075**	**0.100**	**0.200**	**0.500**
	Electrical conductivity of nanocomposites (S cm^{1})				
NFC/RGO/DTAB	$3.12 \times 10^{-8} \pm 9.98 \times 10^{-7}$	$1.11 \times 10^{-6} \pm 1.02 \times 10^{-7}$	$2.56 \times 10^{-5} \pm 1.08 \times 10^{-5}$	$1.28 \times 10^{-4} \pm 9.85 \times 10^{-5}$	$5.44 \times 10^{-5} \pm 1.11 \times 10^{-5}$
NFC/RGO/DDAB	$4.46 \times 10^{-8} \pm 8.96 \times 10^{-7}$	$4.76 \times 10^{-8} \pm 2.78 \times 10^{-7}$	$1.43 \times 10^{-7} \pm 1.43 \times 10^{-8}$	$1.02 \times 10^{-6} \pm 8.73 \times 10^{-7}$	$9.75 \times 10^{-7} \pm 1.29 \times 10^{-7}$
NFC/RGO/SDS	$2.82 \times 10^{-8} \pm 8.45 \times 10^{-9}$	$2.08 \times 10^{-8} \pm 7.98 \times 10^{-10}$	$3.09 \times 10^{-7} \pm 2.86 \times 10^{-8}$	$8.92 \times 10^{-7} \pm 1.30 \times 10^{-7}$	$9.95 \times 10^{-7} \pm 6.78 \times 10^{-8}$
NFC	$1.97 \times 10^{-10} \pm 1.59 \times 10^{-9}$				
NFC/DTAB	$1.78 \times 10^{-9} \pm 9.15 \times 10^{-8}$	$5.83 \times 10^{-9} \pm 2.05 \times 10^{-8}$	$9.82 \times 10^{-9} \pm 6.14 \times 10^{-8}$	$5.94 \times 10^{-9} \pm 7.82 \times 10^{-8}$	$1.37 \times 10^{-9} \pm 8.10 \times 10^{-8}$
NFC/DDAB	$3.23 \times 10^{-9} \pm 1.49 \times 10^{-8}$	$3.67 \times 10^{-9} \pm 4.36 \times 10^{-8}$	$7.32 \times 10^{-9} \pm 5.32 \times 10^{-8}$	$7.62 \times 10^{-9} \pm 4.81 \times 10^{-8}$	$7.17 \times 10^{-9} \pm 8.28 \times 10^{-8}$
NFC/SDS	$6.03 \times 10^{-9} \pm 2.04 \times 10^{-8}$	$5.76 \times 10^{-9} \pm 1.01 \times 10^{-8}$	$9.32 \times 10^{-9} \pm 8.24 \times 10^{-8}$	$8.88 \times 10^{-9} \pm 5.21 \times 10^{-8}$	$9.45 \times 10^{-9} \pm 1.24 \times 10^{-9}$

In general, anionic surfactant SDS, brings only moderate improvements in the electrical properties of GCPs, with the highest conductivity achieved at 9.95 x 10^{-7} S cm^{-1}. Meanwhile, cationic surfactant DTAB improves conductivity by six orders of magnitude, achieving 1.28 x 10^{-4} at surfactant concentration of 0.200 M. There are no surprises to the increasing electrical conductivities on increasing surfactant concentration, as a similar trend was also found elsewhere (Mohamed et al., 2018b; Suriani, Nurhafizah, Mohamed, Zainol, & Masrom, 2015). Interestingly however, the effects of surfactants reaches a limit, as was seen previous literatures (Coleman, 2009; Wang, Yi, & Shen, 2016). The presence of high surfactant concentration in the nanocomposites was presumed to enhance the electrical conductivity of the nanocomposites (Tkalya, Ghislandi, Alekseev, Koning, & Loos, 2010).

A complex picture emerges from the measurements with DDAB surfactant (1.02 x 10^{-6} S cm^{-1}). With a slightly higher carbon number for DDAB, it gives a rather limited electrical conductivity enhancement with only four orders magnitude improvement compared to the neat NFC (1.97 x 10^{-10} S cm^{-1}). It might be expected that longer surfactant tails (higher C – number) will occupy a larger area on the graphene surfaces (Adamczyk, Para, & Warszyński 1999; Manne, Cleveland, Gaub, Stucky, & Hansma, 1994; Matsuo et al., 1999; McCoy et al., 2018; Moulik, Haque, Jana, & Das, 1996). Thus, it could provide a greater barrier to avoid water contact at the graphene surfaces, which may lead to destabilization. However, this is not observed in the current study.

In earlier work, Matsuo and co-workers revealed that the graphite [AZMI IS IT GRAPHITE ORE GRAPHENE?? – CHECK AND CORRECT THIS PLEASE] oxide interlayer distance concurrently increases with surfactant alkyl chain length (Matsuo et al., 1999). This may lessen the tendency of adjacent graphene sheets to

aggregate. It was presumed that the surfactant forms bilayers between the graphite oxide sheets, where longer tails (larger areas occupied by surfactant tails) would hinder dense packing on the GO surfaces. Studying dispersions of graphene with ionic surfactants, Smith and co-workers also noted an improved dispersion stability using a cationic surfactant with higher C – number (Smith, Lotya, & Coleman, 2010). Although the longer tail achieves a lower dispersion concentration, it provides greater stability, after 7 days of observation. This idea again is inconsistent with the trend reported here.

Looking at electrical conductivity of GCPs over all surfactant concentrations, DTAB maintains higher conductivity compared to SDS and DDAB. It therefore can be suggested that the stability of GCP suspensions are sensitive to the chemical structure of hydrophilic moieties of the stabilizing surfactants. The result is in agreement with Quennouz and co-workers who also highlighted the effect of surfactant hydrophilic structure on the stability of surfactant/cellulose nanofibril suspensions, where SDS requires 20-fold higher concentration than DTAB to give the same suspension stability (Quennouz, Hashmi, Choi, Kim, & Osuji, 2016). This phenomenon can also be explained from the viewpoint of RGO and surfactant affinity. McCoy et al. (2018) revealed that the headgroup type is the overriding factor for affinity between surfactants and RGO surfaces, as cationic surfactants proved to be more attractive for RGO surfaces than anionics.

Looking at the conductivity values of GCPs, the results obtained here are over a similar range with other related studies (see Table S2) (Feng, Zhang, Shen, Yoshino, & Feng, 2012; Kiziltas et al., 2016; Wang et al., 2015). Rather than obtaining high conductivity values with a high amount of nanofiller (Wang et al., 2018; Ye et al., 2016), here it is shown that an improvement on the NFC nanocomposite electrical

properties can be expected at considerably low nanofiller contents (see Table S1 and S2) with the help of surfactant. All in all, the cationic DTAB provided significantly higher conductivity enhancement compared to DDAB and anionic SDS. In these systems, when using surfactants with the same alkyl chain length, it seems that cationic surfactants are the best option for the resulting nanocomposite properties.

3.2 Raman spectroscopy of graphite and graphene/NFC paper (GCP)

Raman spectroscopy was used to analyze the structural changes experienced by graphite in GCPs. The prominent peaks of graphene based materials located at 1350 (D-peak) and 1580 cm^{-1} (G-peak) (Ferrari, 2007) are displayed in Fig. 1. The peak positions of each sample are summarized in Table S3 (Supplementary material). Graphite has a negligibly small and weak D-peak. The G-peak located at 1581 cm^{-1} is clearly more intense than the D-peak. As the graphite] was exfoliated, oxidized, and subjected to chemical treatment (reduction process to restore the sp^2-conjugated network), the D and G peak evolve significantly. In the GCPs samples, the D-peak is clearly identifiable with prominent peaks. At the higher wavenumber side (2D area; 2700 cm^{-1}), it can be seen that graphite displayed a single broad peak, while the GCPs have slimmer and less sharp peaks with a bump like region. The existence of the bump like areas might be due to the presence of chemically induced defects during the GCP fabrication process (Kaniyoor & Ramaprabhu, 2012).

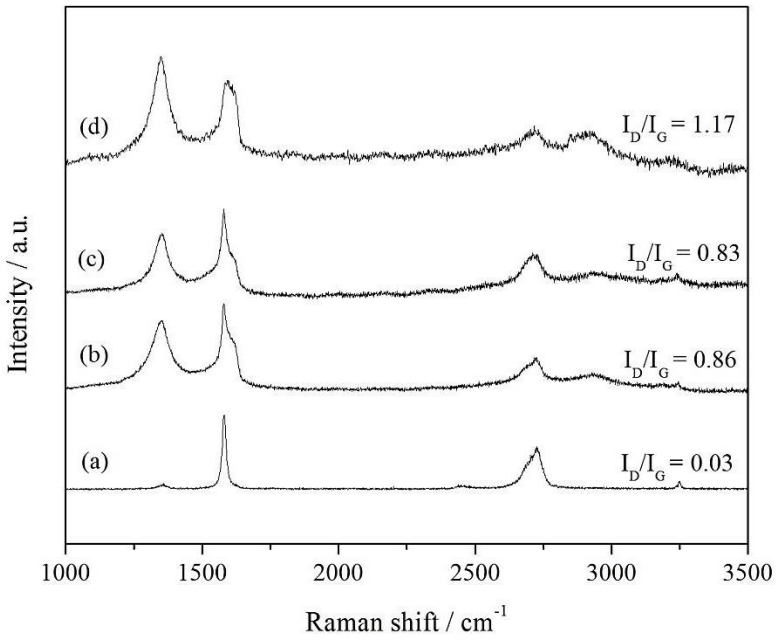

Fig. 1. Raman spectra of the graphite (a) and GCPs stabilized with cationic surfactants: (b) DTAB, (c) DDAB and anionic surfactant: (d) SDS. Surfactant concentration: 0.100 M.

As a consequence of the oxidization and reduction process, the defects increase, leading to an increase in the D-peak intensity (I_D). To characterize the lattice structure of RGO, the ratio of Raman intensities (defect to graphitic ratio; I_D/I_G) was calculated, where lower I_D/I_G indicates lower defects in the graphene structure. As can be seen, the I_D/I_G ratio of graphene presented in the GCP significantly increased compared to the starting material (graphite), implying that the exfoliation and reduction process has been successful (Chua & Pumera, 2013; Kudin et al., 2008). Comparison of I_D/I_G value between the GCPs shows that the sample with SDS gives the highest Raman ratio. The results suggest that RGO in GCPs stabilized by SDS has the highest level of remnant functional groups, and the sp^2-carbon basal plane is less healed during the reduction process compared to DTAB or DDAB. Correlating the I_D/I_G ratio with electrical properties of the GCPs reveals a pattern of higher

conductivity for GCP with lower defect ratios. Here, the choice of surfactant can be linked with the quality of RGO produced during the fabrication process, whereby better surfactants produce RGO with lower defect densities, and thus higher electrical conductivities. Although such trends are noted, it can be seen that the I_D/I_G difference between DTAB and DDAB is close. Hence, more detail is necessary to evaluate factors affecting the different performance of surfactants in this series, particularly for DTAB and DDAB.

3.3 Morphology of graphene/NFC paper (GCP)

The internal structure of RGO dispersions inside NFC matrices was investigated by FESEM. Fig. 2 shows FESEM images of the GCPs as well as the NFC. As shown in Fig. 2a, NFC exhibits a random arrangement of tap-like fibrils having a diameter of 32 – 49 nm without any preferential orientation. In the case of GCPs (Fig. 2b – d), various morphologies of nanofiller can be seen decorating the NFC fibers. Different regions of NFC fibrillated networks can be seen, and RGO can be identified as aggregates (Fig. 2c and d) or more defined stacked layered structures (Fig. 2b).

Comparison of the GCPs morphologies with different surfactants at low magnification images (Fig. 2b – d) revealed that RGOs produced using DTAB and DDAB have considerably larger sizes compared with SDS. GCPs stabilized with DTAB appear to feature large flaked RGO regions, although, closer observation (Fig. 2b') reveals less defined sheets edges with stacked structure. Meanwhile, RGO in GCPs with DDAB (Fig. 2c and c') and SDS (Fig. 2d and d') exist as clumped aggregated structures both in high and low magnification imaging, unlike those observed with DTAB. Based on the FESEM, results it is considered that the RGOs

can be successfully dispersed into the NFC matrices. The results also match well with the trends in electrical conductivity discussed above.

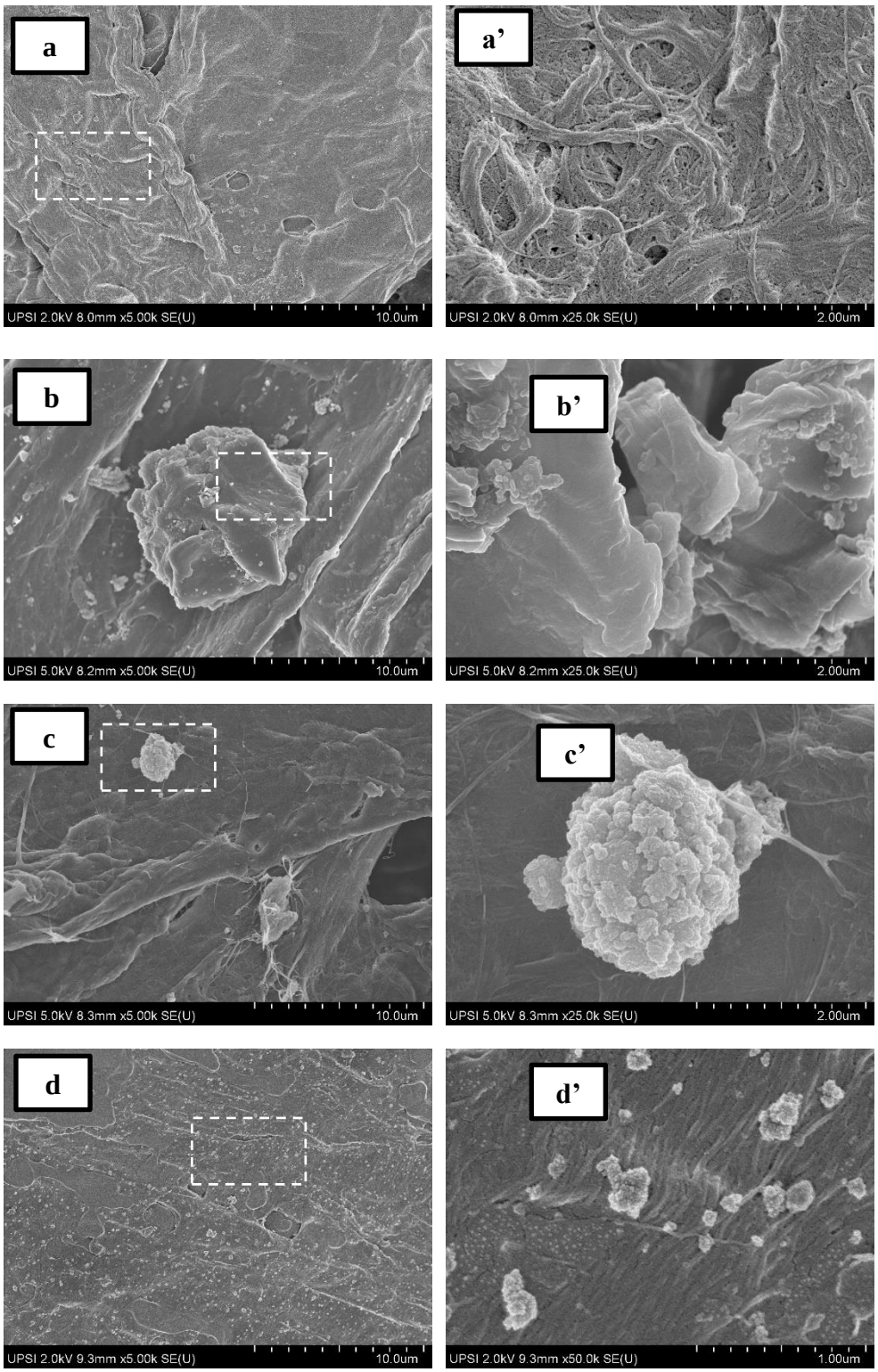

Fig. 2. FESEM images of nanofibrillated kenaf cellulose (NFC) (a and a') and GCP: with DTAB (b and b'), with DDAB (c and c'), and with SDS (d and d'). The selected areas for higher magnification imaging are marked by the dashed squares.

It is known that the electrical conductivity of nanocomposite is affected by the dispersion state of the nanofiller inside the host. In this case, more uniformly distributed nanofillers are expected to give higher electrical conductivities (Mao, Zhu, & Jiang, 2012; Tkalya et al., 2012). In addition to this, the electrical properties also depend on the quality of graphene, in other words, using more exfoliated graphene sheets leads to higher electrical conductivity (Mao et al., 2012). Visualization of the RGOs inside NFC matrices using FESEM revealed different morphologies resulting from different surfactants. From these images it can be deduced that DTAB offers better exfoliation and stabilization than SDS and DDAB, yielding defined flakes rather than clumped aggregated structures.

The results and trends obtained here agreed well with the electrical conductivity measurements described above. However, linking the morphology of the RGOs inside the GCPs does not lead to such obvious trends as for the electrical conductivity measurements. All in all, by comparing the morphology of the GCPs, it is therefore reasonable to assume that DTAB is the best dispersant out of the surfactants used in this study.

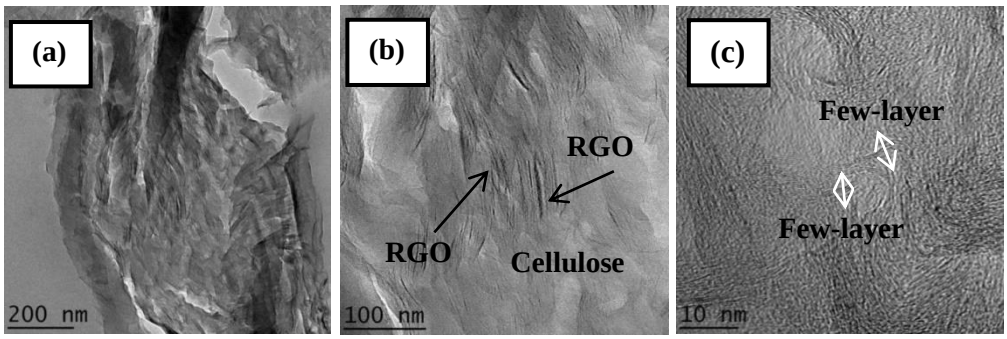

Fig. 3. HRTEM images of the GCP stabilized by DTAB: (a) Typical morphologies at low magnification (b) higher magnification. Grey areas are NFC fibers. Note that many RGO sheets are embedded throughout the NFC matrix (c) Edge view of RGO sheets.

FESEM images have highlighted the different RGO morphologies dispersed in NFC matrices. In order to understand the embedded microstructure of RGO inside NFC stabilized by DTAB surfactant, an ultrathin section of GCP was observed under HRTEM. Observations at low magnification (Fig. 3 (a and b) indicate the presence of RGO (dark lines), supporting the FESEM images. An enlarged view (Fig. 3c) revealed that RGO was present as few-layer sheets. Hence, it is seen that DTAB is a good surfactant for this application.

3.4 Studying the role of surfactant for dispersion stability: Zeta (ζ)-potential measurements

In aqueous dispersions, the electrical double layer is an important feature and zeta potential measurements are useful to asses stability (Hunter, 1981). Addition of electrolytes may affect the distribution of surface charge, depending on the nature of added component. Efforts to make a comparison with literature values however are restricted due to the very limited number of studies focused on colloidal stability of these related systems.

To provide understanding of the surfactant stabilization and its relationship, if any, to the efficiencies in elevating the composite properties, the zeta potentials of

RGO dispersions stabilized by DTAB, DDAB, and SDS are given in Table 3. The RGO dispersion quality and the ability of surfactant to ensure stabilization scales very well with the measured zeta potentials. The sign of zeta potential (negative or positive) reflects the type of surfactant adsorbed onto the material. As a rule of thumb, system with a zeta potential of |10 – 20| mV is close to the threshold of agglomeration whereas a value of |30| mV is accepted for colloidal stability (Lotya et al., 2009).

Between the cationic surfactants, although DTAB displayed a zeta potential above the standard of stable colloidal system +32 mV, its cousin DDAB exhibited a zeta potential of +23 mV which can be classified as less stable. In contrast to the results obtained here, Smith et al. noted very good graphene dispersion stability with quaternary ammonium bromide surfactants (> +45 mV) (Smith et al., 2010). Interestingly, SDS clearly outperforms DTAB and DDAB in terms of electrical barrier strength, displaying a zeta potential value of -43 mV.

Looking only at the results from zeta potential measurements, SDS is considered to offer significantly more stability than DTAB and DDAB, and so SDS should offer better electrical properties than both cationic surfactants. The results from the electrical conductivity measurements in Table 2 however did not follow this order. Perhaps there are other factors why the reinforcing factor of RGO with SDS is attenuated. Intermolecular interactions between each component: RGO, surfactants, and NFC therefore need to be further investigated to explain the behavior. These observations may facilitate better understanding for selecting more suitable surfactant types for the development of conductive papers of nanocellulose and graphene.

3.5 Effect of headgroup type on surfactant aggregation structure: small-angle neutron scattering (SANS) study of surfactant solutions and reduced graphene oxide (RGO)-stabilized surfactant systems

Surfactants will self-assemble into micelles in the aqueous phase driven by the tendency of hydrophobic tails to minimize contact with water. When carbon nanomaterials are also present, surfactants can adsorb on the surfaces in various configurations (Lin et al., 2016; Tkalya et al., 2012; Vaisman, Wagner, & Marom, 2006). Thus, it is important to describe how the surfactants organize on RGO surfaces, and for this small angle neutron scattering (SANS) studies have been conducted. SANS studies can give quantitative information about the shape and size of the surfactant aggregation structures in aqueous phases and in RGO dispersions. Such information will contribute to understanding the interactions between RGO and surfactants, as well as provide insight into the structure and nature of the adsorbed surfactant layers.

Fig. 4 shows SANS profiles for the surfactant solutions and RGO dispersions with DTAB, DDAB, and SDS. The scattering intensity *I(Q)* typically is related to nanostructure: the features contributing to *I(Q)* are shape and size of the particles, usually described as particle form factor *P(Q)*. With charged particle dispersions, the scattering profile is also affected by inter-particle interactions which can be either attractive or repulsive in nature, accounted for by the structure factor *S(Q)*. For more detailed discussions on SANS, readers are directed elsewhere (Feigin & Svergun, 1987; Hollamby, 2013).

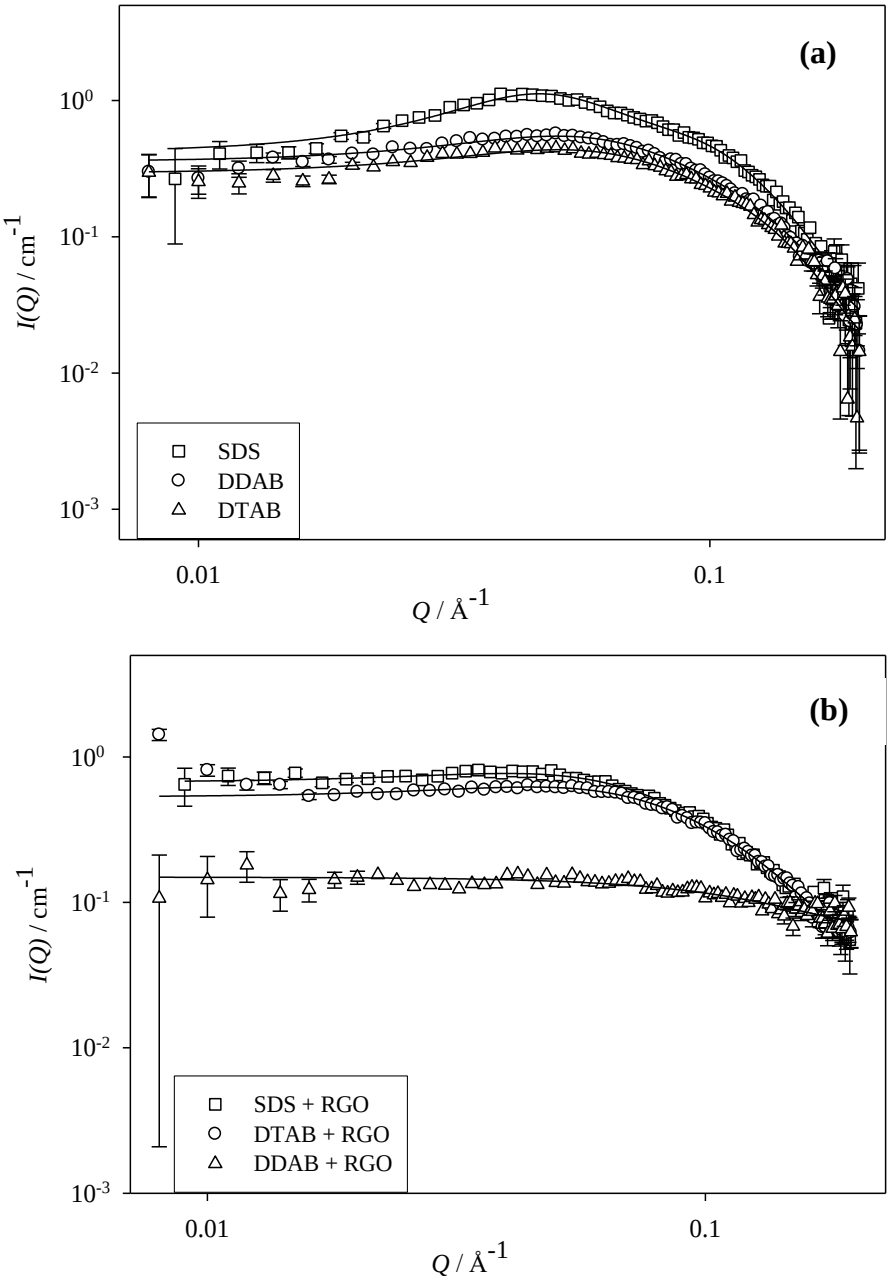

Fig. 4. SANS profiles for (a) DTAB, DDAB, and SDS solutions and (b) the RGO dispersions. [surfactant] = 0.030 M and T = 25 °C. Lines are model fits for charged spherical or ellipsoidal micelles with the Hayter-Penfold *S(Q)*) model. Characteristic error bars are shown for the lowest intensity samples.

Table 3

Model fit parameters for SANS data[a]

Sample	ζ-potential (mV)	Model	R_{sphere} (Å)	R_a (Å)	X ± 0.2
DTAB	-	Ellipsoid	-	15.0	1.5
DDAB	-	Ellipsoid	-	11.0	2.2
SDS	-	Sphere	22.0		
DTAB + RGO	+32 ± 1	Ellipsoid	-	14.0	1.7
DDAB + RGO	+23 ± 1	Sphere	17.0	-	-
SDS + RGO	-43 ± 4	Sphere	24.0	-	-

[a][surf.] = 0.030 M. Charged micelles were fitted with interparticle structure factor *S(Q)* for Hayter-Penfold model

For SDS, the scattering profile agrees well with a model for charged spherical micelles, consistent with literature (Paul et al., 2005; Yurekli, Mitchell, & Krishnamoorti, 2004). The interparticle interaction was fitted to a Hayter-Penfold *S(Q)* model (Hayter & Penfold, 1983), with the fit parameters listed in Table 3 Data analysis through scattering law fitting gives the micellar radius R_{sphere} to be 22.0 Å, consistent with previous works (Magid, Li, & Butler, 2000; Mohamed et al., 2018a; Wang et al., 2016; Yurekli et al., 2004).

Measurements with the cationic surfactant DTAB gave *I(Q)* characteristic of ellipsoidal micelles experiencing repulsive interactions, modelled by the Hayter-Penfold interparticle factor, *S(Q*). An axial micelle radius, R_a, of 15.0 Å was obtained with an aspect ratio, *X,* 1.5 indicating that the micelles are oblate spherical ($R_a < R_b$). The result is in concordant with literature values where the radius lie between 15.0 to

19.0 Å at surfactant concentration of 0.02 – 0.20 M (Brown et al., 2012; Griffith & Notley, 2012; Mahajan, Vohra, Kaur, & Aswal, 2008; McCoy et al., 2018). Bergstorm and Pederssen (1998, 1999) also revealed the aggregation of ellipsoidal micelles, although in their study, the structure factor *P(Q)* is more suited to the tri-axial ellipsoidal model.

The scattering profile with DDAB surfactant is also indicative of an ellipsoidal form factor, with a peak owing to the electrostatic interparticle stabilization of micelles. Fitting the SANS data give an axial radius of 11.0 Å with an ellipsoidal axis ratio 2.2. It seems that the secondary axis of DDAB is larger compared to that for the DTAB surfactant. This increase in micellar radius can be attributed to the length of the surfactant tail. Previous SANS experiments on cationic ammonium halide surfactants revealed an increase of micellar radii with longer hydrophobic tails (Aswal & Goyal, 1998; Berr, 1987; McCoy et al., 2018).

Parallel SANS experiments with the same surfactant concentration in D_2O were conducted, and the results are compared to those for pure surfactant solutions to reveal any structural changes when RGO is incorporated. There is no substantial difference in scattering over the *Q* range, compared with the pure surfactant solutions. Hence, the curves can be adequately fitted with the ellipsoidal and spherical models as appropriate. As can be referred in Table 3, the micellar dimensions are broadly the same for DTAB and SDS. This is surprising for DTAB, as it is the most efficient surfactant in the series. A micelle shape transition, or changes in dimensions, are to be expected when such low dimensional material is added to the system, as those found in the existing literature (Granite, Radulescu, & Cohen, 2012; McCoy et al., 2018; Wang et al., 2004). McCoy et al. found significant differences in the scattering profile in the low *Q* region (0.003 – 0.02 Å), following the Q^{-2} indicative of planar flat RGO

sheets, which was not found in this study (McCoy et al., 2018). In contrast, DDAB transitioned into different micellar shape, and an ellipsoidal to spherical transition was observed. If only considering the axial radius of ellipsoids, the presence of RGO resulted in a larger micellar radius 17.0 Å. In general, although analysis of the SANS data revealed physically realistic parameters, it is rather challenging to draw a firm trend or pattern on the self-assembly of the surfactants on RGO surfaces.

The existing literature suggests certain arrangements of surfactant molecules on graphene surfaces as characteristic of positive surfactant – graphene interactions, hence the aggregation structure will adopt hemi-micelles, or cylindrical structures (for the case of CNTs) (Lin et al., 2016; Lin, Shih, Strano, & Blankschtein, 2011; Matarredona et al., 2003). With this picture in mind, it can be suggested that the interactions of dodecyl tails and graphene surfaces are less favorable. The surfactants are presumed to just randomly adsorb on graphene surface, enough to prevent the adjacent neighboring RGO sheets from aggregating and destabilizing.

3.6 Comparison of cationic vs. anionic surfactants at graphene and NFC interfaces: A proposed mechanism

A significant advancement in studying the adsorption of surfactant at carbon nanomaterial surfaces has been the use of small-angle neutron scattering and molecular dynamic simulations (Lin et al., 2011; McCoy et al., 2018; Wang, 2009). With these techniques, insight into how the surfactant adsorbs can be obtained. In this study, the cationic DTAB came out as the most efficient for stabilizing the RGO/NFC composites. Interestingly, although the zeta potential is suggestive of a “stable dispersion”, SANS data do not show any structural changes for the micellar properties, giving a relatively similar micelle radius. General observations on

colloidal characterization (SANS and zeta-potential) showed that although giving higher conductivity enhancement, DTAB still behaves in a similar fashion with the SDS and DDAB.

There is strong evidence on the relationship between stability and the tendency of surfactants to follow the curvature of dispersed materials (Matarredona et al., 2003; Vaisman et al., 2006; Wang, 2009; Wang et al., 2004). However, this is not the case here; therefore, a model of surfactant fully-covered graphene surfaces as has been used to explain aggregation behavior in a previous study (Mohamed et al., 2018a,b) must be ruled out here.

In an earlier study, Yurekli et al. (2004) assumed a structureless random adsorption of SDS on single walled carbon nanotube (SWCNT) walls being responsible for the aqueous phase dispersion stability. This stems from the constant micelle shape and size upon SWCNT addition. Instead of adopting cylindrical micelles, SDS molecules were suggested to adsorb at the graphene sheets of CNTs randomly with no preferential arrangement. This picture be used to explain the behavior of all the surfactants used in this study. A schematic figure of the surfactant self-assembly is now given in Fig. 5.

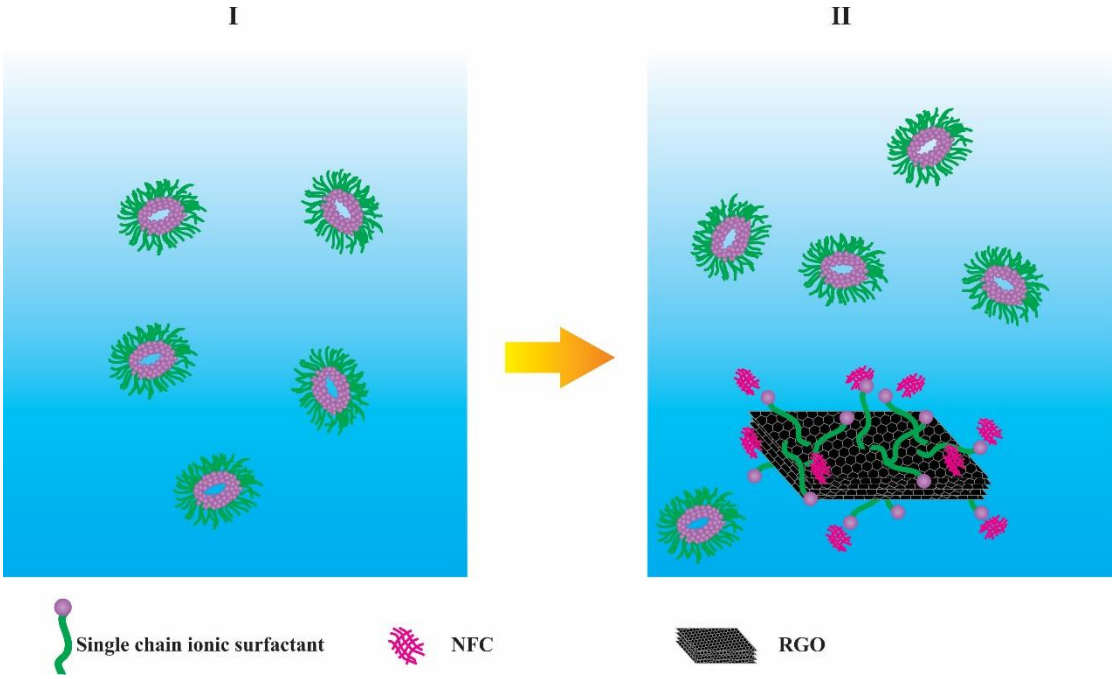

Fig. 5. Proposed mechanism of ionic dodecyl surfactant arrangement in RGO/NFC composites.

In the stable dispersions surfactant may exist as individual molecules, in micelles or adsorbed to graphene surfaces (Sa & Kornev, 2011; Wang et al., 2004). The ideal situation is that the surfactant fully wraps the graphene surfaces, minimizing contact with water, hence adopting the shape of graphene either as stacked disk or stacked bilayer aggregates. This can be achieved when the attractions between surfactant tails or headgroups and graphene surfaces are strong enough. In this case, the interaction between the surfactants and graphene surfaces may be less favorable, hence the limited number of surfactant monomers adsorbed on graphene surfaces (McCoy et al., 2018; Wang, Han, Wang, Qin, & Guo, 2008).

The surfactant tails are thought to adsorb perpendicularly toward graphene surfaces, or lying flat to maximize the hydrophobic interactions with no preferential adsorption site (Fig. 5 (II)). The charged headgroups are expected to face toward the aqueous phase and interact with the hydrophilic segments of nanocellulose

(Bandyopadhyay, Shelley, Tarek, Moore, & Klein, 1998; Ducker & Grant, 1996; Shah, Chiu, & Sinnott, 2006; Wang et al., 2008). Due to the limited adsorbed surfactant on graphene, hence the surfactant molecules do not form aggregation structures on top of graphene surface, in turn; the associated surfactant in micelles dominates the aqueous phase. This may explain the absence of micellar structural transitions in the presence of graphene as observed by SANS.

It has been widely suggested that anionic surfactants are more efficient for stabilizing graphene dispersions (Lin et al., 2016; Shih, Lin, Strano, & Blankschtein, 2015; Smith et al., 2010; Texter, 2014). Notley (2012), however proved otherwise. Using a continuous surfactant addition approach, cationic surfactants (CTAB, DTAB, TTAB) were revealed to be on a par with anionic surfactant (SDS) in terms of produced dispersed graphene concentration. In the graphene dispersion literature (Texter, 2014), when the surfactant comprises similar long carbon chains, it is actually very difficult to say which of the stabilizers is better, as different works lead to different conclusions.

It is known that the positioning of surfactants at an interface between water and another phase is a result of an interfacial energy minimization for the surfactant, water and graphene (Coleman, 2009). Therefore, the ability of surfactants to provide stabilization may be assessed through surfactant geometrical considerations, namely fractional free volume (FFV) (Stone, Smith, da Rocha, Rossky, & Johnston, 2004). This concept was initially introduced to understand the design of effective surfactants for microemulsion studies (Mohamed et al., 2010). As such it is used to quantify the bulkiness of surfactants at an interface, hence the space available for interpenetration between two incompatible materials can be assessed. In polymer science, free volume

is important parameter to define the permeability of polymers. Here, the FFV is defined in Equation (1) as

$$\mathrm{FFV} = 1 - \frac{V}{tA_h} \quad (1)$$

Where, V is the volume of a surfactant tail, t is the thickness of the interface, and A_h is the interfacial area per headgroup. To implement a succinct discussion, the justification made for the FFV calculation as well as detail of each parameter is given in Supplementary Material (Table S4 and S5). It is hypothesized that lower FFV will minimize the penetration of water at graphene surfaces, hence giving higher conductivity of the GCPs.

As can be seen in Table S6, surfactant performance in stabilizing RGO and NFC dispersions, that is optimum electrical conductivity, does show a general trend with FFV. The electrical conductivity in fact increases as FFV decreases. Lower FFV should favor a lower area for water penetration on graphene surfaces and thus greater dispersion stability. In support of this interpretation, analysis using fluorescence spectroscopy revealed that the void space near DTAB headgroup is less than around SDS, suggesting larger water permeability with SDS (Karukstis, Suljak, Waller, Whiles, & Thompson, 1996). Calculation of headgroup surface area through modeling also revealed larger area occupied by DTAB than SDS (Karukstis et al., 1996). In general, the results show that the surfactant performance at graphene – water interface correlates with FFV.

As well as surfactant structure and architecture, it is interesting to consider the influence of surfactant activity for stabilizing these composites. A recent review has summarized extensive work on the interaction of cationic and anionic surfactants with nanocellulose (Tucker, Petkov, Penfold, & Thomas, 2012). The nature of surfactant

adsorption onto NFC surfaces is broadly similar to other hydrophilic/hydrophobic solid surfaces; except there is an additional aspect to be considered arising from cellulose swelling (Tucker et al., 2012).

By measuring the adsorption isotherm, Biswas and Chattoraj (1997) proposed that the interaction between homologous ammonium halide surfactant involved hydrophobic interactions between surfactant tails and cellulose surfaces (Biswas & Chattoraj, 1997). Meanwhile, based on the adsorption of CTAB onto anionic nanofibrillated cellulose, others have postulated that the formation of surfactant bilayers switches the cellulose nanofibrils to be more hydrophilic (Xhanari, Syverud, Chinga-Carrasco, Paso, & Stenius, 2011). The interaction was suggested to be driven by electrostatic interactions between anionic carboxyls present in the nanofibrils with the positively charged CTAB headgroups. Using SDS, Tucker et al. observed the adsorption of surfactant molecules toward the hydrophilic part of negatively charged cellulose at concentrations greater than 2×10^{-3} M (Tucker et al., 2012). Others have proposed the formation of bridging-mediated fibrous networks between SDS and negatively charged nanofibrils (Quennouz et al., 2016). Such networks can be induced by the presence of favorable, albeit weak, interactions between groups in SDS and negatively charged species in cellulose nanofibrils. These studies proved that regardless of the headgroup type, ionic surfactants will be able to display affinity with cellulose surfaces.

Tardy et al. (2017) listed plausible reasons why cationic surfactants outperform anionics for stabilizing these dispersions. The rate of anionic surfactant adsorption at the cellulose-water interface was said to be lower than that of cationic surfactants (Paria, Manohar, & Khilar, 2004). Even when compared to other surfactant types, the kinetics are the fastest and the forces of interaction are the

strongest between cellulosic materials and cationic surfactants (Tardy et al., 2017). Studying the rheology of cellulose nanofibrils, Quennouz and co-workers noted that DTAB needed only approximately one eighth of the SDS concentration to form homogeneous clear gel suspensions (Quennouz et al., 2016). The underlying reason for the higher DTAB efficiency, and for cationic surfactants in general, is possibly increased affinities between surfactants and nanocellulose surfaces, facilitating the dispersion of RGO inside NFC matrices.

4. Conclusions

The advantages in utilizing electrochemical approaches to produce dispersed reduced graphene oxide (RGO) have already established (Parvez et al., 2014; Suriani et al., 2016; Suriani et al., 2015). Our previous study has shown that it is possible to obtain electrically conductive NFC paper stabilized by specialized ionic liquid-type surfactants (Mohamed et al., 2018a). Here, more common readily available commercial surfactants are employed instead, and effects of headgroup chemistry with two model ionic surfactants –anionic and cationic - was investigated in terms of dispersion stability, electrical conductivity enhancement, and aggregation properties. There is a distinct graphene-compatibility of the anionic and cationic surfactants, with DTAB being the most efficient stabilizer. Although the chemical structures between DTAB and DDAB differ by only substitution of a headgroup ethyl moiety in place of a methyl group, it is still not clear why DDAB does not perform as well as its homologue DTAB. Considering these two analogues have very similar solution properties (Fisicaro, Biemmi, Compari, Duce, & Peroni, 2007), DDAB would be expected to give similar dispersion stability as DTAB.

One way to consider adsorption is in terms of adsorption and surface aggregation structures (Mohamed et al., 2018a,b; Tkalya et al., 2012; Vaisman et al., 2006). The strength and type of interfacial interaction can be expected to influence the morphology of aggregates formed on RGO surfaces. Nevertheless, here a similar micelle structure was seen in both the aqueous solutions and RGO dispersions. The stabilization mechanism was then proposed to be random adsorption of surfactant molecules on graphene surfaces, co-existing with the background surfactant micelles. Because the surfactants bear the same C12 hydrophobic tails, it is reasonable to assume that the any changes in adsorption and stabilization are a result of hydrophilic headgroup structure. A readily calculated surfactant parameter, namely FFV is seen to be useful for describing the different behavior between anionic and cationic surfactants. A decrease in FFV favors a more stable system and thus higher electrical conductivity of the composites. The results underline that the choice of surfactant headgroup significantly affects the affinity with RGO and nanocellulose.

Acknowledgements

The work funded under grants from Universiti Pendidikan Sultan Idris Rising Star Research Grant (Grant Code: 2019-0118-103-01). This project was supported by JSPS [KAKENHI, Grant-in-Aid for Young Scientists (A), No. 23685034], KAKENHI, Grant-in-Aid for Scientific Research (B), No. 26289345, Fund for the Promotion of Joint International Research (Fostering Joint International Research) No. 15KK0221, Grant-in-Aid for Challenging Research (Exploratory), No.17K19002] and Leading Research Organizations (RCUK [through EPSRC EP/I018301/1], ANR [13-G8ME-0003]) under the G8 Research Councils Initiative for Multi-lateral Research Funding—G8-2012. The authors thank the Science and Technology

Facilities Council for allocation of beam time, travel and consumables (experiment number RB1710004). This work benefited from the use of the SasView application, originally developed under NSF Award DMR-0520547. SasView also contains code developed with funding from the EU Horizon 2020 programme under the SINE2020 project Grant No 654000.

References

Adamczyk, Z., Para, G., & Warszyński , P. (1999). Influence of ionic strength on surface tension of cetyltrimethylammonium bromide. *Langmuir, 15*, 8383-8387.

Aswal, V. K., & Goyal, P. S. (1998). Mixed micelles of alkyltrimethylammonium halides a small-angle neutron-scattering study. *Physica B: Condensed Matter, 245*, 73-80.

Bandyopadhyay, S., Shelley, J. C., Tarek, M., Moore, P. B., & Klein, M. L. (1998). Surfactant aggregation at a hydrophobic surface. *The Journal of Physical Chemistry B, 102*, 6318-6322.

Bergström, M., & Pedersen, J. S. (1998). Small-angle neutron scattering (SANS) study of aggregates formed from aqueous mixtures of sodium dodecyl sulfate (SDS) and dodecyltrimethylammonium bromide (DTAB). *Langmuir, 14*, 3754-3761.

Bergström, M., & Pedersen, J. S. (1999). Structure of pure SDS and DTAB micelles in brine determined by small-angle neutron scattering (SANS). *Physical Chemistry Chemical Physics, 1*, 4437-4446.

Berr, S. S. (1987). Solvent isotope effects on alkytrimethylammonium bromide micelles as a function of alkyl chain length. *Journal of Physical Chemistry, 91*, 4760-4765.

Biswas, S. C., & Chattoraj, D. K. (1997). Polysaccharide-surfactant interaction. 1. Adsorption of cationic surfactants at the cellulose-water interface. *Langmuir, 13*, 4505-4511.

Brown, P., Bushmelev, A., Butts, C. P., Cheng, J., Eastoe, J., Grillo, I., Heenan, R. K., & Schmidt, A. M. (2012). Magnetic control over liquid surface properties with responsive surfactants. *Angewandte Chemie International Edition, 124*, 2464-2466.

Chua, C. K., & Pumera, M. (2013). Reduction of graphene oxide with substituted borohydrides. *Journal of Materials Chemistry A, 1*, 1892-1898.

Coleman, J. N. (2009). Liquid-phase exfoliation of nanotubes and graphene. *Advanced Functional Materials, 19*, 3680-3695.

Ducker, W. A., & Grant, L. M. (1996). Effect of substrate hydrophobicity on surfactant surface-aggregate geometry. *The Journal of Physical Chemistry, 100*, 11507-11511.

Feigin, L. A., & Svergun, D. I. (1987). *Structure analysis by small-angle X-ray and neutron scattering*. (1st ed). New York: Springer, (Chapter 1).

Feng, Y., Zhang, X., Shen, Y., Yoshino, K., & Feng, W. (2012). A mechanically strong, flexible and conductive film based on bacterial cellulose/graphene nanocomposite. *Carbohydrate polymers, 87*, 644-649.

Ferrari, A. C. (2007). Raman spectroscopy of graphene and graphite: Disorder, electron-phonon coupling, doping and nonadiabatic effects. *Solid State Communications, 143*, 47-57.

Fisicaro, E., Biemmi, M., Compari, C., Duce, E., & Peroni, M. (2007). Thermodynamics of aqueous solutions of dodecyldimethylethylammonium bromide. *Journal of Colloid and Interface Science, 305*, 301-307.

Georgakilas, V., Otyepka, M., Bourlinos, A. B., Chandra, V., Kim, N., Kemp, K. C., Hobza, P., Zboril,R., & Kim, K. S. (2012). Functionalization of graphene: covalent and non-covalent approaches, derivatives and applications. *Chemical Reviews, 112*, 6156-6214.

Granite, M., Radulescu, A., & Cohen, Y. (2012). Small-angle neutron scattering from aqueous dispersions of single-walled carbon nanotubes with Pluronic F127 and poly (vinylpyrrolidone). *Langmuir, 28*, 11025-11031.

Griffith, A., & Notley, S. M. (2012). pH dependent stability of aqueous suspensions of graphene with adsorbed weakly ionisable cationic polyelectrolyte. *Journal of Colloid and Interface Science, 369*, 210-215.

Hayter, J. B., & Penfold, J. (1983). Determination of micelle structure and charge by neutron small-angle scattering. *Colloid & Polymer Science, 261*, 1022-1030.

Hollamby, M. J. (2013). Practical applications of small-angle neutron scattering. *Physical Chemistry Chemical Physics, 15*, 10566-10579.

Hou, M., Xu, M., & Li, B. (2018). Enhanced electrical conductivity of cellulose nanofiber/graphene composite paper with a sandwich structure. *ACS Sustainable Chemistry & Engineering, 6*, 2983-2990.

Hunter, R. J. (1981). *Zeta potential in colloid science: principles and applications*. (1st ed.). London: Academic Press, (Chapter 2).

Kaniyoor, A., & Ramaprabhu, S. (2012). A Raman spectroscopic investigation of graphite oxide derived graphene. *AIP Advances, 2*, 032183.

Karukstis, K. K., Suljak, S. W., Waller, P. J., Whiles, J. A., & Thompson, E. H. Z. (1996). Fluorescence analysis of single and mixed micelle systems of SDS and DTAB. *The Journal of Physical Chemistry, 100*, 11125-11132.

Kiziltas, E. E., Kiziltas, A., Rhodes, K., Emanetoglu, N. W., Blumentritt, M., & Gardner, D. J. (2016). Electrically conductive nano graphite-filled bacterial cellulose composites. *Carbohydrate polymers, 136*, 1144-1151.

Kudin, K. N., Ozbas, B., Schniepp, H. C., Prud'Homme, R. K., Aksay, I. A., & Car, R. (2008). Raman spectra of graphite oxide and functionalized graphene sheets. *Nano Letters, 8*, 36-41.

Lin, S., Shih, C.-J., Sresht, V., Rajan, A. G., Strano, M. S., & Blankschtein, D. (2016). Understanding the colloidal dispersion stability of 1D and 2D materials: perspectives from molecular simulations and theoretical modeling. *Advances in Colloid and Interface Science, 244*, 36-53.

Lin, S., Shih, C.-J., Strano, M. S., & Blankschtein, D. (2011). Molecular insights into the surface morphology, layering structure, and aggregation kinetics of surfactant-stabilized graphene dispersions. *Journal of the American Chemical Society, 133*, 12810-12823.

Lotya, M., Hernandez, Y., King, P. J., Smith, R. J., Nicolosi, V., Karlsson, L. S., Blighe, F. M., De, S., Wang, Z., McGovern, I. T., Duesberg, G. S., & Coleman, J. N. (2009). Liquid phase production of graphene by exfoliation of graphite in surfactant/water solutions. *Journal of the American Chemical Society, 131*, 3611-3620.

Magid, L. J., Li, Z., & Butler, P. D. (2000). Flexibility of elongated sodium dodecyl sulfate micelles in aqueous sodium chloride: a small-angle neutron scattering study. *Langmuir, 16*, 10028-10036.

Mahajan, R. K., Vohra, K. K., Kaur, N., & Aswal, V. K. (2008). Organic additives and electrolytes as cloud point modifiers in octylphenol ethoxylate solutions. *Journal of surfactants and detergents, 11*, 243-250.

Manne, S., Cleveland, J. P., Gaub, H. E., Stucky, G. D., & Hansma, P. K. (1994). Direct visualization of surfactant hemimicelles by force microscopy of the electrical double layer. *Langmuir, 10*, 4409-4413.

Mao, C., Zhu, Y., & Jiang, W. (2012). Design of electrical conductive composites: tuning the morphology to improve the electrical properties of graphene filled immiscible polymer blends. ACS Applied Materials & Interfaces, 4, 5281-5286.

Matarredona, O., Rhoads, H., Li, Z., Harwell, J. H., Balzano, L., & Resasco, D. E. (2003). Dispersion of single-walled carbon nanotubes in aqueous solutions of the anionic surfactant NaDDBS. *The Journal of Physical Chemistry B, 107*, 13357-13367.

Matos, C. F., Galembeck, F., & Zarbin, A. J. G. (2014). Multifunctional and environmentally friendly nanocomposites between natural rubber and graphene or graphene oxide. *Carbon, 78*, 469-479.

Matsuo, Y., Niwa, T., & Sugie, Y. (1999). Preparation and characterization of cationic surfactant-intercalated graphite oxide. *Carbon, 37*, 897-901.

McCoy, T. M., de Campo, L., Sokolova, A. V., Grillo, I., Izgorodina, E. I., & Tabor, R. F. (2018). Bulk properties of aqueous graphene oxide and reduced graphene oxide with surfactants and polymers: adsorption and stability. *Physical Chemistry Chemical Physics, 20*, 16801-16816.

Mohamed, A., Ardyani, T., Abu Bakar, S., Brown, P., Hollamby, M., Sagisaka, M., & Eastoe, J. (2016). Graphene-philic surfactants for nanocomposites in latex technology. *Advances in Colloid and Interface Science, 230,* 54-69.

Mohamed, A., Ardyani, T., Abu Bakar, S., Sagisaka, M., Umetsu, Y., Hamon, J. J., Rahim, B. A., Esa, S. R., Abdul Khalil, H. P. S., Mamat, M. H., King, S., & Eastoe, J. (2018b). Rational design of aromatic surfactants for graphene/natural rubber latex nanocomposites with enhanced electrical conductivity. *Journal of Colloid and Interface Science, 516*, 34-47.

Mohamed, A., Ardyani, T., Abu Bakar, S., Sagisaka, M., Umetsu, Y., Hussin, M. R. M., Ahmad, M. K., Mamat, M. H., King, S., Czajka, A., Hill, C., & Eastoe, J. (2018a). Preparation of conductive cellulose paper through electrochemical exfoliation of graphite: The role of anionic surfactant ionic liquids as exfoliating and stabilizing agents. *Carbohydrate polymers, 201,* 48-59.

Mohamed, A., Trickett, K., Chin, S. Y., Cummings, S., Sagisaka, M., Hudson, L., Nave, S., Dyer, R., Rogers, S., Heenan, R. K., & Eastoe, J. (2010). Universal Surfactant for Water, Oils, and CO_2. *Langmuir, 26*, 13861-13866.

Moulik, S. P., Haque, M. E., Jana, P. K., & Das, A. R. (1996). Micellar properties of cationic surfactants in pure and mixed states. *The Journal of Physical Chemistry, 100*, 701-708.

Nguyen Dang, L., & Seppälä, J. (2015). Electrically conductive nanocellulose/graphene composites exhibiting improved mechanical properties in high-moisture condition. *Cellulose, 22*, 1799-1812.

Paria, S., Manohar, C., & Khilar, K. C. (2004). Effect of cationic surfactant on the adsorption characteristics of anionic surfactant on cellulose surface. *Colloids and Surfaces A: Physicochemical and Engineering Aspects, 232*, 139-142.

Parvez, K., Wu, Z.-S., Li, R., Liu, X., Graf, R., Feng, X., & Müllen, K. (2014). Exfoliation of graphite into graphene in aqueous solutions of inorganic salts. *Journal of the American Chemical Society, 136*, 6083-6091.

Paul, A., Griffiths, P. C., Pettersson, E., Stilbs, P., Bales, B. L., Zana, R., & Heenan, R. K. (2005). Nuclear magnetic resonance and small-angle neutron scattering studies of anionic surfactants with macrocounterions: tetramethylammonium dodecyl sulfate. *The Journal of Physical Chemistry B, 109*, 15775-15779.

Peng, H., Meng, L., Niu, L., & Lu, Q. (2012). Simultaneous reduction and surface functionalization of graphene oxide by natural cellulose with the assistance of the ionic liquid. *The Journal of Physical Chemistry C, 116*, 16294-16299.

Quennouz, N., Hashmi, S. M., Choi, H. S., Kim, J. W., & Osuji, C. O. (2016). Rheology of cellulose nanofibrils in the presence of surfactants. *Soft Matter, 12*, 157-164.

Sa, V., & Kornev, K. G. (2011). Analysis of stability of nanotube dispersions using surface tension isotherms. *Langmuir, 27*, 13451-13460.

Shah, K., Chiu, P., & Sinnott, S. B. (2006). Comparison of morphology and mechanical properties of surfactant aggregates at water-silica and water-graphite interfaces from molecular dynamics simulations. *Journal of Colloid and Interface Science, 296*, 342-349.

Shih, C.-J., Lin, S., Strano, M. S., & Blankschtein, D. (2015). Understanding the stabilization of single-walled carbon nanotubes and graphene in ionic surfactant aqueous solutions: large-scale coarse-grained molecular dynamics simulation-assisted DLVO theory. *The Journal of Physical Chemistry C, 119*, 1047-1060.

Smith, R. J., Lotya, M., & Coleman, J. N. (2010). The importance of repulsive potential barriers for the dispersion of graphene using surfactants. *New Journal of Physics, 12*, 125008.

Stone, M. T., Smith, P. G., da Rocha, S. R. P., Rossky, P. J., & Johnston, K. P. (2004). Low interfacial free volume of stubby surfactants stabilizes water-in-carbon dioxide microemulsions. *Journal of Physical Chemistry B, 108*, 1962-1966.

Suriani, A. B., Nurhafizah, M. D., Mohamed, A., Masrom, A. K., Sahajwalla, V., & Joshi, R. K. (2016). Highly conductive electrodes of graphene oxide/natural rubber latex-based electrodes by using a hyper-branched surfactant. *Materials & Design, 99*, 174-181.

Suriani, A. B., Nurhafizah, M. D., Mohamed, A., Zainol, I., & Masrom, A. K. (2015). A facile one-step method for graphene oxide/natural rubber latex nanocomposite production for supercapacitor applications. *Materials Letters, 161*, 665-668.

Tardy, B. L., Yokota, S., Ago, M., Xiang, W., Kondo, T., Bordes, R., & Rodes, O. J. (2017). Nanocellulose-surfactant interactions. *Current Opinion in Colloid & Interface Science, 29*, 57-67.

Texter, J. (2014). Graphene dispersions. *Current Opinion in Colloid & Interface Science, 19*, 163-174.

Tkalya, E. E., Ghislandi, M., Alekseev, A., Koning, C., & Loos, J. (2010). Latex-based concept for the preparation of graphene-based polymer nanocomposites. Journal of Materials Chemistry, 20, 3035-3039.

Tkalya, E. E., Ghislandi, M., de With, G., & Koning, C. E. (2012). The use of surfactants for dispersing carbon nanotubes and graphene to make conductive

nanocomposites. *Current Opinion in Colloid & Interface Science, 17*, 225-232.

Tucker, I. M., Petkov, J. T., Penfold, J., & Thomas, R. K. (2012). Interaction of the anionic surfactant SDS with a cellulose thin film and the role of electrolyte and poyelectrolyte. 2 Hydrophilic cellulose. *Langmuir, 28*, 10223-10229.

Vadukumpully, S., Paul, J., & Valiyaveettil, S. (2009). Cationic surfactant mediated exfoliation of graphite into graphene flakes. *Carbon, 47*, 3288-3294.

Vaisman, L., Wagner, H. D., & Marom, G. (2006). The role of surfactants in dispersion of carbon nanotubes. *Advances in Colloid and Interface Science, 128-130*, 37-46.

Wang, F., Drzal, L. T., Qin, Y., & Huang, Z. (2015). Multifunctional graphene nanoplatelets/cellulose nanocrystals composite paper. *Composites Part B: Engineering, 79*, 521-529.

Wang, H. (2009). Dispersing carbon nanotubes using surfactants. *Current Opinion in Colloid & Interface Science, 14*, 364-371.

Wang, H., Zhou, W., Ho, D. L., Winey, K. I., Fischer, J. E., Glinka, C. J., & Hobbie, E. K. (2004). Dispersing single-walled carbon nanotubes with surfactants: a small angle neutron scattering study. *Nano Letters, 4*, 1789-1793.

Wang, Q., Han, Y., Wang, Y., Qin, Y., & Guo, Z.-X. (2008). Effect of surfactant structure on the stability of carbon nanotubes in aqueous solution. *The Journal of Physical Chemistry B, 112*, 7227-7233.

Wang, R., Bian, H., Ji, H., & Yang, R. (2018). Preparation of lignocellulose/graphene composite conductive paper. *Cellulose*, *25*, 6139-6149.

Wang, S., Yi, M., & Shen, Z. (2016). The effect of surfactants and their concentration on the liquid exfoliation of graphene. *RSC Advances*, *6*, 56705-56710.

Xhanari, K., Syverud, K., Chinga-Carrasco, G., Paso, K., & Stenius, P. (2011). Reduction of water wettability of nanofibrillated cellulose by adsorption of cationic surfactants. *Cellulose, 18*, 257-270.

Xiong, R., Hu, K., Grant, A. M., Ma, R., Xu, W., Lu, C., Zhang, X., & Tsukruk, V. V. (2016). Ultrarobust transparent cellulose nanocrystal-graphene membranes with high electrical conductivity. *Advanced Materials, 28*, 1501-1509.

Ye, Y.-S., Zeng, H.-X., Wu, J., Dong, L.-Y., Zhu, J.-T., Xue, Z.-G., Zhou, X.-P., Xie, X.-L., & Mai, Y.-W. (2016). Biocompatible reduced graphene oxide sheets with superior water dispersibility stabilized by cellulose nanocrystals and their polyethylene oxide composites. *Green Chemistry, 18*, 1674-1683.

Yurekli, K., Mitchell, C. A., & Krishnamoorti, R. (2004). Small-angle neutron scattering from surfactant-assisted aqueous dispersions of carbon nanotubes. *Journal of the American Chemical Society, 126*, 9902-9903.

Zhang, X., Liu, X., Zheng, W., & Zhu, J. (2012). Regenerated cellulose/graphene nanocomposite films prepared in DMAC/LiCl solution. *Carbohydrate polymers*, *88*, 26-30.

Zhou, J., & Zhang, L. (2000). Solubility of cellulose in NaOH/urea aqueous solution. *Polymer Journal*, *32*, 866-870.